ADVANCED MATERIALS TECHNOLOGIES
www.advmattechnol.de

A Silver Nanowires-Based Flexible Capacitive Touch Screen in Tactile Displays for Individuals with Visual Impairment Using Gesture Recognition

Ahmed Hamza, Sara Alzalabny, Priyanka Buduru, Sagar Bhagwat, Ali Usama, Santosh Kumar Prabhulingaiah, Qingchuan Song, Sebastian Kluck, Gerhard Jaworek, Pegah Pezeshkpour, and Bastian E. Rapp*

Capacitive touch screens (CTS's) are essential components in most of today's digital devices. However, for the visually impaired (VI) users due to the uneven topography of the tactile surface, CTS's are more challenging to implement and thus this field remains largely underdeveloped. Considering the limited space around the microactuators driving the typical Braille dots for a tactile screen with ten dots-per-inch (dpi) resolution, the materials used for CTS should be flexible and durable with high mechanical strength. In this work, a flexible CTS based on polyimide (PI) and silver nanowires (AgNWs) as electrodes with a total thickness of 210 µm is developed. The dimensions of the AgNWs are on average 7.9 ± 2.4 µm in length and 85 ± 24 nm in width. The AgNWs electrodes showed low resistance and good adhesion to the PI substrate. A gesture recognition application is collected from the capacitive data to classify different gestures (including single- and double-click, swipe-left and -right, scroll-up and -down as well as zoom-in and -out) with two different approaches; machine learning and deep learning are implemented. The best performance is obtained using the YOLO model with a high validation accuracy of 97.76%. Finally, a software application is developed with the proposed hand gestures in real-time to foster interaction of VI users with the tactile display allowing them to navigate a Windows file system and interact with the documents via hand gestures in a similar manner as sighted users on a conventional touch display will be able to do. This work paves the way to utilize CTS for the tactile displays in the market developed for VI users.

1. Introduction

In the digital world today, hand-held touch-screen electronics are ubiquitous and inevitable part of daily life activities. Apple, one of the many suppliers of touch-screen electronics, announced that it alone had shipped 135.3 million tablets (iPads) in 2023.[1] However, the market for tactile displays for individuals with visual impairment, (VI) with a total affected population of ≈2.2 billion is significantly smaller than the market reported for sighted users.[2] This is while the cost for small refreshable tactile screens is at least three times more than a conventional display amounting to around a few tens of thousand euros in the EU market.[3,4] Most of the tablets developed for the VI are Braille-text systems integrated with basic features such as speech-generating or audio self-prompting systems as well as browsers or dedicated voice synthesizers, all of which lack true interactive communication with a VI user.[5] To promote equality for the VI and to contribute to their equity and accessibility to portable tablets, the tablet must be

A. Hamza, S. Alzalabny, P. Buduru, S. Bhagwat, A. Usama, S. K. Prabhulingaiah, Q. Song, S. Kluck, P. Pezeshkpour, B. E. Rapp
Laboratory of Process Technology
NeptunLab
Department of Microsystem Engineering (IMTEK)
University of Freiburg
79110 Freiburg im Breisgau, Germany
E-mail: Pegah.Pezeshkpour@neptunlab.org

The ORCID identification number(s) for the author(s) of this article can be found under https://doi.org/10.1002/admt.202401029

DOI: 10.1002/admt.202401029

A. Hamza, S. Bhagwat, B. E. Rapp
Freiburg Materials Research Center (FMF)
University of Freiburg
Stefan-Meier-Straße 21, 79104 Freiburg im Breisgau, Germany

S. Alzalabny, G. Jaworek
ACCESS@KIT
Karlsruhe Institute of Technology
76131 Karlsruhe, Germany

A. Usama, Q. Song, B. E. Rapp
Cluster of Excellence livMatS@ FIT – Freiburg Center of Interactive Materials and Bioinspired Technologies
University of Freiburg
Georges-Köhler-Allee 105, 79110 Freiburg im Breisgau, Germany

developed with a touch (tactile) screen embedded with the Braille dots actuated with advanced technologies. Due to the presence of the Braille dots, manufacturing such tactile displays, with a touch screen on its outermost layer, does not align with the current technologies of touch smartphones or tablets.[6] Although many researchers have focused on making touch screens viable for the VI, it is still a cumbersome process. Current technologies of a Braille-embedded touch screen are still limited to basic functions and mechanisms for the Braille input such as: localization, i.e., identifying the current location of the fingers for activating or deactivating sections of the display, selection of a text, object, file, or folder by single or double-click, navigation by swiping left or right, or scrolling up and down, and zoom in/out on the text, graphics, and graphs.

These functions are implemented in the majority of Braille input technologies like TypeIn–Braille,[7] Edge–Braille,[8] and Braille-Enter[9] as text-based inputs. Graphics are not supported on these devices. Despite the current high-resolution displays in the market, the displays for the VI have a resolution (taxel pitch) of 10-dpi or slightly higher, which makes them more challenging to display graphics due to the reduced resolution.

For the regular touch screens for sighted users, several technologies to implement touch functionality have been developed. In brief, the single or multiple-touch approaches mainly include *resistive touch screens (RTS)* which consist of two layers of conductive materials, separated by a thin insulating layer.[10] Touch creates contact between the resistive layers and has mostly been implemented using conductive ceramics such as, e.g., Indium Tin Oxide (ITO). While ITO is an excellent candidate in touch screens, it is hard, fragile, and fabricated via sputtering technique at high temperatures and vacuum processes.[11] Alternatives to ITO in resistive touch screens are carbon nanotubes (CNT) electrodes,[12] reduced graphene oxide (rGO),[13] or transparent conductive inks consisting of poly(3,4-ethylenedioxythiophene) doped with poly(4-styrenesulfonic acid) (PEDOT:PSS) electrodes. These techniques mainly suffer from the complex manufacturing process for the CNT dispersion, the low conductivity of rGO, and the acidity and batch-to-batch variation of PEDOT:PSS.[14,15] Another common approach uses *optical infrared* (IR) via Light Emitting Diodes (LED's) and photodetector cameras. Its main drawbacks are related to the high number of transmission diodes and photodiodes, as well as the scanning speed and transmission distance of IR light.[16] In addition to RTS and IR technologies, *surface acoustic wave (SAW)* including transducers have been investigated which can convert electrical signals to ultrasonic waves absorbed by a finger touching the screen but are easily affected by the environmental parameters.[17] While all these techniques are implemented in regular touch displays, their implementation in Braille tactile displays is challenging. This is due to the architecture of these displays with Braille pins in place which makes both the selection of the material and its fabrication technology more challenging. Among the various techniques, *capacitive* technology promises the most stringent integration into the architecture of Braille-embedded touch screens with the potential of high sensitivity, durability, multi-touch support, and possibilities for large-size screens. In addition to ITO, several materials have been used in developing capacitive touch technology including conductive polymers like polypyrrole, silver nanowires, graphene nanoplatelets, carbon nanotubes as well as carbon nanofibers.[18–23] While many of these materials are ideal for stretchable electronics, their complex fabrication procedure makes them more difficult to integrate with Braille tactile displays.

The aim of the work at hand was twofold. First, to develop efficient touch screens that can be conveniently implemented on the structured matrices of conventional Braille dot systems. In addition to conductive polymers, several materials have been reported in the literature for conductive and flexible (micro/-nano) fibers such as silver-doped spider silk fiber fabricated through spinning,[24] silver polymer elastomer film membranes,[25] or polyaniline NWs,[26] which could not easily be integrated with the Braille displays due to their fabrication technology or complicated synthesis process. For this, we identified silver nanowires (AgNWs) as competent candidates for the generation of highly electrically conductive and elastic polymer coatings that can be queried for touch events. They possess excellent optical, electrical, magnetic, and thermal properties, which have been explored for a wide range of applications in transparent and flexible electronics and touch screens.[27–29] In this work, we demonstrate the implementation of an AgNW-enabled device using a tactile display with 15 × 15 Braille dots. Second, as identifying touch events on such a matrix is of limited use to VI users, we wanted to provide a holistic approach for gesture recognition on this hardware, thus paving the way for complex and versatile input devices for VI users. Among all the communication assistive technologies in performing daily life activities of VI users, including speech systems[30] or auditory aid,[31] gesture recognition systems are key to improving the interface with the device.[5,32] Toward interpreting reliable recognition of gestures, deep learning (DL) and machine learning (ML) were identified as promising tools with high potential in distinguishing the gestures.[33,34] ML approaches significantly enhance the detectability of gestures during touchscreen interaction, particularly in the case of tactile displays where the surface texture is rough and the continuity of lines is challenging to maintain. Thus, being able to detect gestures will be a key element in empowering the next generation of aid and support tools for the VI.

In summary, this work demonstrates a novel and easy-to-scale approach to capacitive touch sensor surfaces for Braille displays using a 15 × 15 dot Braille display. We furthermore demonstrate a DL and ML-based approach to provide holistic gesture recognition including single- and double-click, swipe-left and -right, scroll-up and -down as well as zoom-in and -out on this device. We believe that this work will be an essential and easy-to-apply building block for future interactive devices for the VI.

2. Results and Discussion

2.1. System Design

Tactile displays for VI consist of taxels (tactile pixels or Braille dots) on a tactile surface (i.e., screen) as shown in **Figure 1**. There are various ways to actuate the individual Braille dots but the technology developed in this work is independent from the type of actuation.[35–42] For a tactile display with a CTS, the arrangement of capacitive electrodes is limited to the space between the taxels. The mutual capacitive sensing method used in this work is

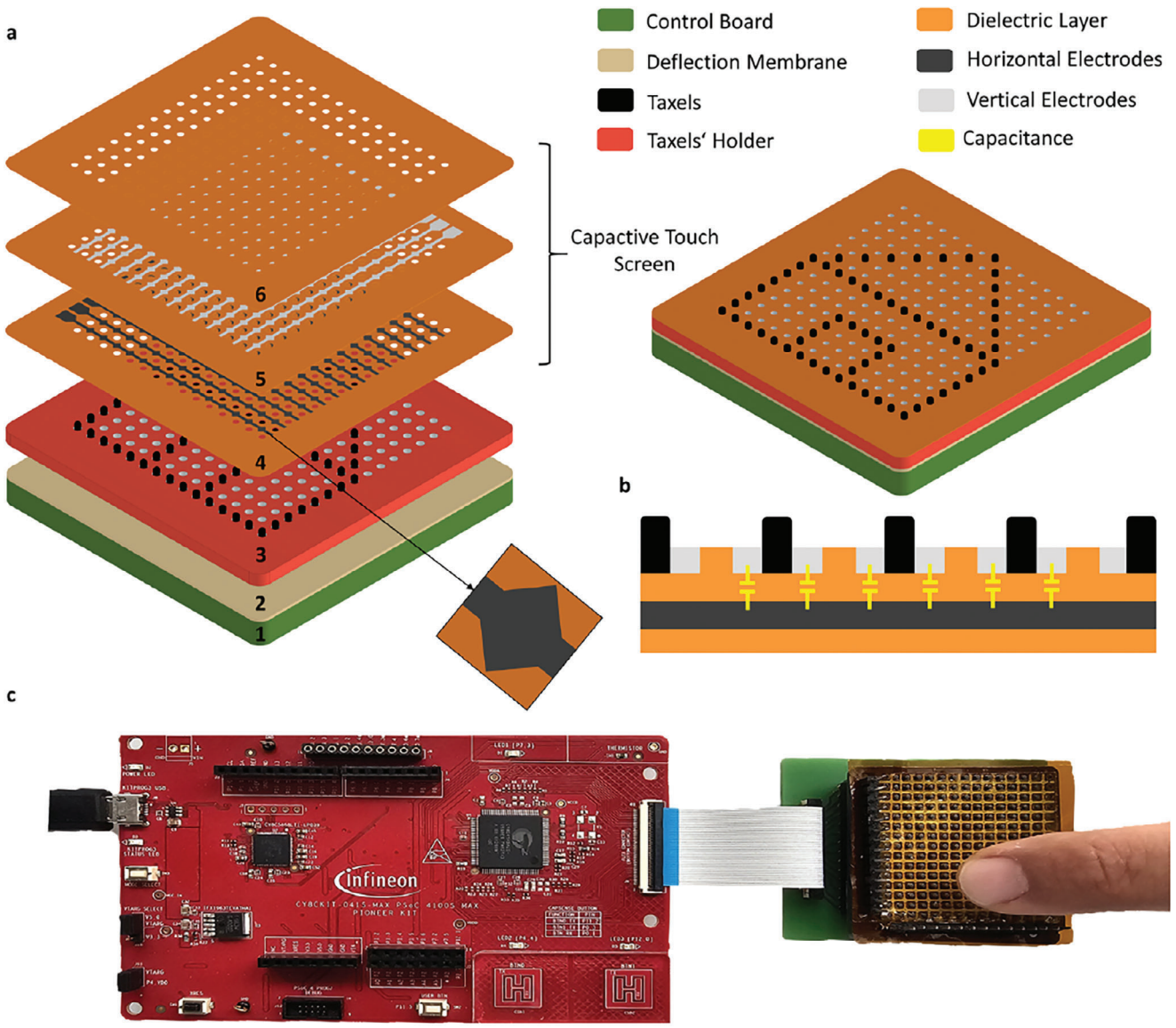

Figure 1. Schematic diagram of a capacitive touch screen (CTS) on the tactile display used as the experimental setup. a) Isometric view of the tactile display. b) Side-view of the CTS. c) Experimental setup of the CTS with the expansion board for data collection and gesture recognition.

designed for a multi-touch display for identifying a set of gestures performed on the screen. The tactile display (Figure 1a) consists of six layers: 1) the control board as the base of the display supporting the actuation of the dots; 2) a deflection membrane acting as the interlayer mechanism between the actuators and the taxels; 3) the taxels as the direct interface which are placed in a holder frame; 4,5) the CTS screen including two dielectric layers with horizontal and vertical electrodes respectively topped with the outmost touch screen layer; 6) a protective layer to cover the electrodes. The diamond-shaped electrodes for the horizontal and vertical traces were stacked on top of each other. When a finger is placed on the taxels, the capacitance between the horizontal and vertical electrodes changes and thus object detection is triggered. Figure 1b shows the side-view of the capacitive layers with a total thickness of 210 µm. The experimental setup used in this work is shown in Figure 1c, the expansion board is connected to the capacitive layers through a flex connector to an FR4-based printed circuit board (PCB) for data collection.

Fabrication of a CTS on a tactile display is challenging as the display consists of taxels that need to penetrate the top layer as a tactile output to the user. For a 10-dpi display, the touch screen must thus consist of a grid of holes for the Braille dots with ≈1.2 mm diameter and a pitch of 2.54 mm on all layers. However, the fabrication of a mechanically stable layer across the dots is challenging for most of the materials commonly used in touch screen technology. Among all the candidates, polyimide (PI) being a well-known material due to its thermal and mechanical stability, was the material selected for the capacitive layer in the current work. It is commercially available in foil thickness in the micrometer range and can be conveniently microstructured using laser micromachining. The most challenging problem to overcome is the choice of the conductive layer often including metal

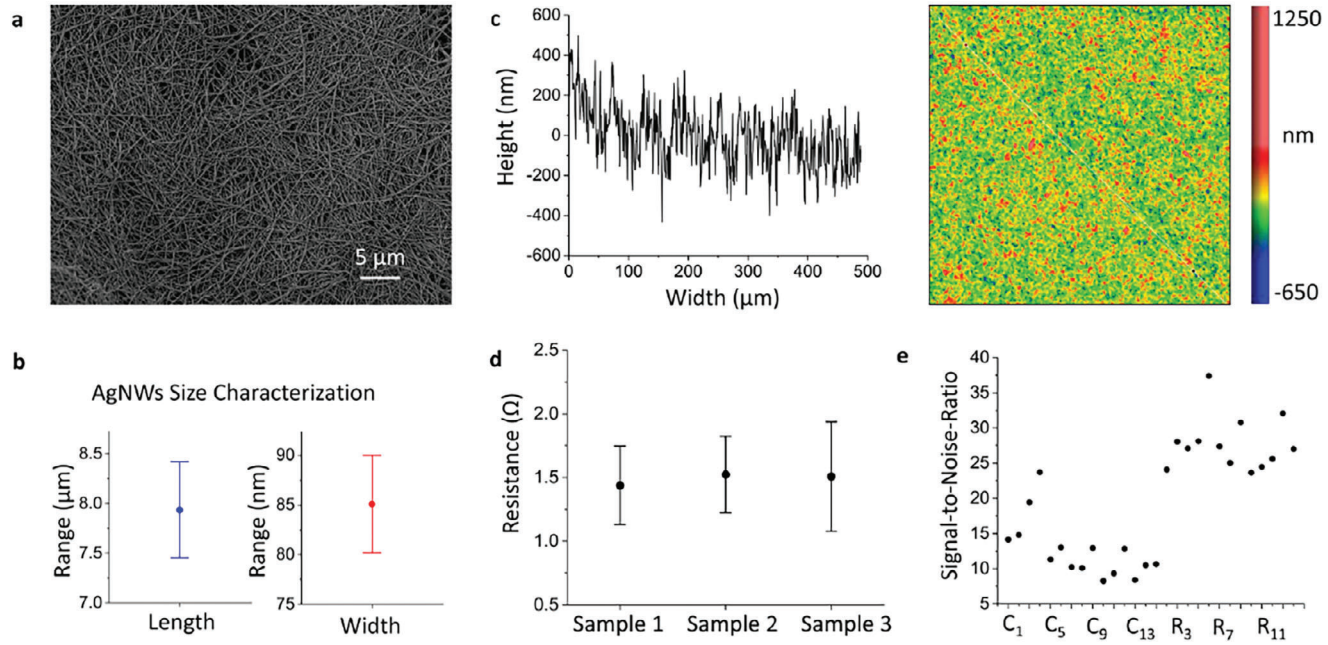

Figure 2. The characterization of the capacitive touch display. a) SEM image of AgNWs after synthesis. b) Size characterization of AgNWs with an average length of 7.9 ± 2.4 µm and an average width of 85 ± 24 nm. c) Surface roughness of the patterned AgNWs on PI using WLI (S_a = 0.11 µm, S_q = 0.14 µm and S_z = 1.922 µm). d) The resistance test of the AgNWs electrodes of three samples using the 4-probe measurement setup. e) Signal-to-noise (SNR) values of each electrode before and after touch (C: Column $_{n\ electrode}$ and R: Row $_{n\ electrode}$) demonstrating values above five which is considered to be a good performance.

electrodes. However, metal electrodes on flexible substrates like PI have to be flexible and must provide good interface bonding to the substrate to prevent delamination and thus device failure. Moreover, the electrodes must show high conductivity, specifically as they are generally mechanically loaded repetitively as a consequence of the taxel actuation. In this work, we chose AgNWs due to the fact that they offer high conductivity and flexibility as well as good adhesion to PI. Synthesis of AgNWs can be costly and time-consuming and several methods have been reported in the literature for fabrication of AgNWs including template methods,[43] electrochemical reduction,[44,45] and wet chemical synthesis[46] as well as electrospinning[47] drop casting,[48] capillary printing,[49] spray coating,[50] inkjet printing,[51] and screen printing.[52] In this work, we chose to synthesize the AgNWs in polyol at a lower reaction temperature which yielded AgNWs with high electrical conductivity, low roughness, and excellent bending stability.[53,54] The Validation of the correct synthesis of high-aspect-ratio AgNWs approaching aspect ratios of 100 and above was carried out using SEM analysis with a scanning electron microscope TESCAN AMBER X SEM machine (TESCAN GmbH, Germany). **Figure 2a** shows an SEM image of AgNWs after synthesis, clearly indicating nanowires without defects and impurities. Image analysis was conducted using ImageJ software to determine the length and the width of the wires where hundreds of random wires were examined. The average length and width of the AgNWs were determined to be 7.9 ± 2.4 µm and 85 ± 24 nm respectively, which indicates a narrow distribution of AgNWs (Figure 2b). The synthesis process of AgNWs plays a key role in the overall yield. In order to obtain an accurate calculation of the yield; three batches of AgNWs were synthesized. The average yield of AgNWs obtained from our process was 82.7% ± 2.22%, which is comparable to the high yield reported in literature ranging between 80% and 90%.[55–58] After the synthesis process, the paste was diluted with ethanol to allow the spreading of AgNWs on the PI substrates to create the electrode pattern. The surface of the resulting electrodes was examined using a white light interferometer (WLI). An arithmetic mean height (S_a) of 0.11 µm, a root mean square height (S_q) of 0.14 µm, and a maximum height (S_z) of 1.92 µm were determined. Figure 2c shows the surface topography of a 500 × 500 µm^2 path and its respective height map. The uniform distribution and the low surface roughness of the AgNWs on the PI substrate demonstrate a successful patterning process with very high accuracy. The polyvinylpyrrolidone (PVP) for synthesizing the AgNWs using the polyol process serves as a capping agent for the nanowires. This AgNWs paste has low surface tension, hence a high wettability. Since PI has high surface energy, dispersing AgNWs on the PI substrate would result in strong interaction between them.[59] To validate the adhesion of the AgNWs, a PI tape was fixed on the electrodes, and pull tests were performed (See Video S1, Supporting Information), showing no defect or delamination of the AgNWs from the PI material. To assess the electrical conductivity of the AgNWs electrodes, we measured the resistance using a four-point probe method (Figure S1a, Supporting Information). By lowering the lever, the four probes were allowed to touch the electrodes and a current (I) of ≈12 mA was applied to three PI samples for ten measurements per sample. The calculated average resistance from the measured voltage (V) of the three samples (Figure 2d) is ≈1.5 ± 0.7 Ω demonstrating a very reliable and high conductivity of the electrodes. To test the durability of the flexible electrodes,

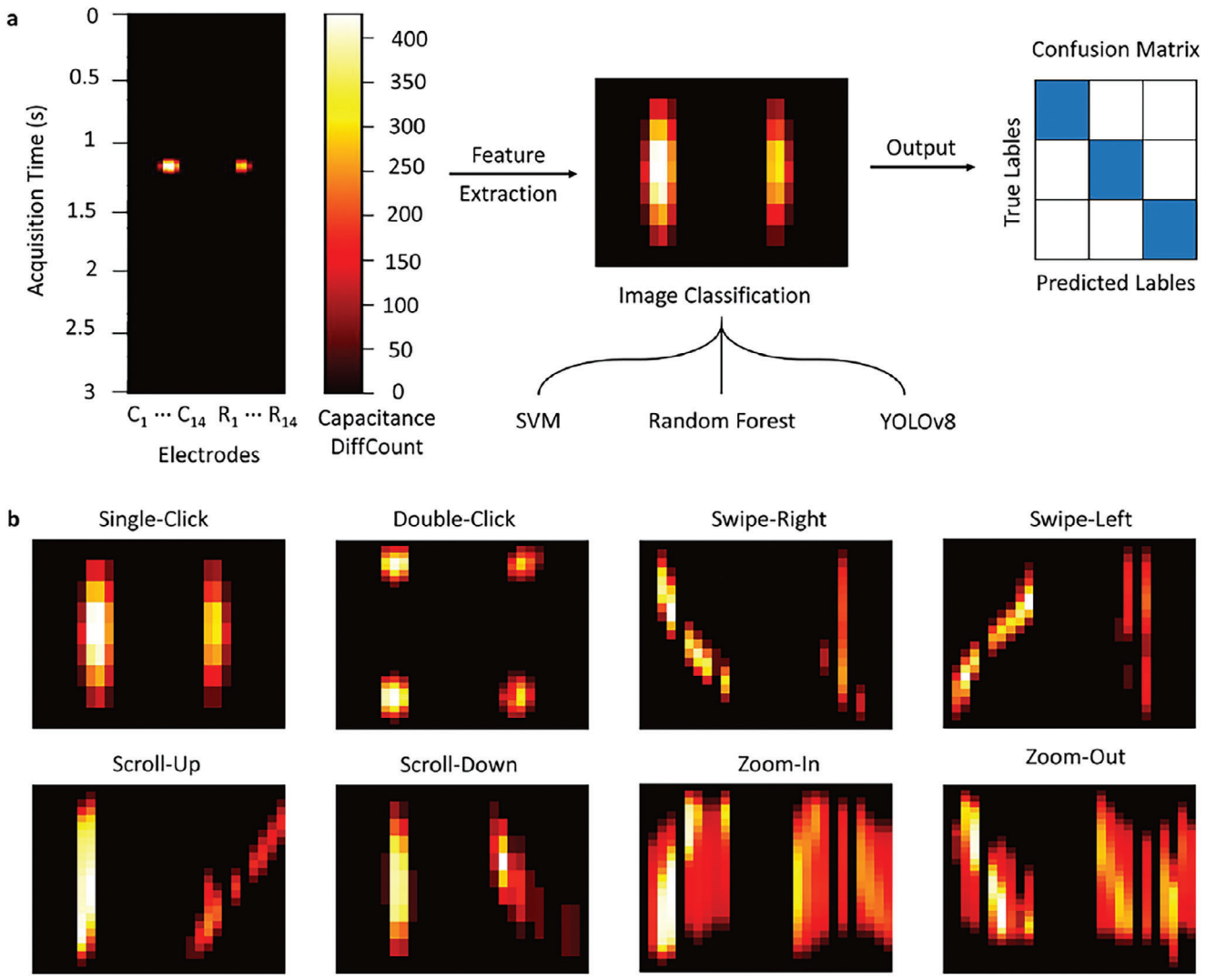

Figure 3. ML and DL approaches to gesture recognition on the developed system. a) The heat map of each electrode over time for 14 columns and 14 rows represented as C1 to C14, and R1 to R14 respectively. After image classification using ML and DL approaches, the resulting accuracy and confusion matrix are derived. b) The input images of all eight investigated gestures on which the models were trained.

the PI substrate with AgNWs was bent several times and no electrode deformation was observed (See Video S1, Supporting Information).

In order to assess the electrodes' potential for capacitive sensing, we carried out a performance and sensitivity test for each electrode before and after human touch by measuring the signal-to-noise ratio (SNR) of the capacitance change. As shown in Figure 2e, the SNR was measured for both rows (horizontal electrodes) and columns (vertical electrodes). According to the design guide of the expansion board, the SNR threshold should exceed 5 to ensure a reliable operation by maintaining a clear distinction between touch and no touch.[60] The results showed all the electrodes have SNR values above this limit with some exceeding values of 30. A disparity of the average SNR values is observed between the rows and the columns, which arises from the electrode's placement in different layers. The further the electrode to the finger touch, the less exposed to the external noise like electromagnetic interference (EMI), hence, the lower the SNR values.[61]

2.2. Data Analysis and Gesture Recognition

Before running the classification model, a preprocessing of the data is required to put the raw data in a comprehensible format to train on. The electrode grid consists of 14 rows and 14 columns. The raw data was collected through the capacitive expansion board over 3 s. with a sampling frequency of 60 Hz, hence 180 data points per electrode. For each measurement, there are 5040 data points for the 28 electrodes in the display. Due to the nature of the raw data, it was presented in an image format in the form of a heatmap with an *x*-axis for the electrodes and the *y*-axis for the time as depicted schematically in **Figure 3a**. The features were extracted for each measurement and the images were cropped

for the duration of the present gesture. Then the images were resized and normalized for a specific dimension of 800 × 600 pixels to have a consistent image size per gesture in data collection. The data normalization ensures the stability of the produced images, if any degradation happens to the capacitive values, although the AgNWs are sandwiched between PI tapes for higher durability. The gestures were classified using two methods: conventional ML approaches and DL approaches. From both, accuracies and confusion matrices were compared. The data and feature extraction were repeated for all gestures and the resulting heatmaps are shown in Figure 3b. The heatmaps show clearly distinguishable patterns for each gesture. In total, we trained the system for eight different gestures: single- and double-click, swipe-left and -right, scroll-up and -down as well as zoom-in and -out.

We chose two popular approaches for ML: *Support Vector Machine* (SVM) and *Random Forest* both of which are common choices in ML due to their high accuracy on relatively small datasets.[62–67] This makes these methods particularly suitable for our system as they require significantly less data required for classification problems. Whereas SVM seeks to find the best hyperplane to separate the data points with different classes (here, the gestures), Random Forest approaches are based on creating an ensemble of decision trees each of which is constructed independently. The final prediction is obtained via a voting process. To implement both SVM and Random Forest algorithms, the images were flattened to a 1D array containing 784 data points for each image. All the data sets from all gestures were concatenated into one matrix and the target value was added to the last column of the dataset for each gesture. Two methods were used to evaluate each model's performance. The first method was the *Train-Test-Split*, where the data was split into an 80% training dataset and a 20% test dataset. Since the dataset consists of a total of 2400 measurements for all gestures in the current work (**Figure** 4a), the training dataset was set to 1920 measurements and the test dataset was set to 480 measurements. The test accuracy was thus assessed and the confusion matrix was deducted, where it provides the individual accuracy of each gesture by comparing the model's predictions for each gesture against the true occurrences of those gestures (Figure 4b,d,e). The second method was *fivefold cross-validation*, where the data is split into fivefolds. One fold was used for testing and the remaining data was used for training. The process was repeated four more times with different folds and the accuracy was determined as the average performance of all folds. This method helps to avoid overfitting resulting in a more robust model. The hyperparameters tuning was conducted through the *Grid Search* method and the best hyperparameters were used for model training. For Random Forest, the training accuracy was 98.9%, the resulting cross-validation accuracy was 95.1%, and the test accuracy was 94.38%. The resulting confusion matrix is shown in Figure 4b. A graphical representation of the receiver operating characteristic (ROC) curve is presented in Figure 4c to examine the performance of the Random Forest algorithm. The figure shows an excellent performance which clearly distinguishes between the gesture classes.

For the SVM, the training accuracy was 99.6%, the resulting cross-validation accuracy was 94.5%, the test accuracy was 95.4% and the resulting confusion matrix is shown in Figure 4d.

In addition to ML approaches, we also investigated DL models focusing on *YOLOv8* (You Only Look Once) as a powerful model that is used for object detection as well as classification problems.[68–70] It is based on *Convolutional Neural Networks* (CNNs) for image processing. CNNs consist of multiple hidden layers that include a convolutional layer, a pooling layer, and fully-connected layers that aim to extract meaningful patterns from input images.[71–73] In our work, we labeled the images and did a *Train-Test-Split*, where the data as well were split into 80% for the training set and 20% for the validation set. The model was training the model only for 20 epochs. The resulting validation accuracy was 97.76%, the confusion matrix is shown in Figure 4e. The confusion matrices show that the algorithms were able to correctly classify all eight gestures with very few misclassifications. The model performance was further examined through the training/validation curves presented in Figure 4f, where the graph shows a continuous decrease of the losses over the epoch indicating a high performance for the model learning.

2.3. Real-Time Implementation Application

The aim of this work was to demonstrate a fully functional gesture recognition system implemented both in hardware and software to be used with tactile displays for VI. In order to verify the successful implementation of the proposed model in a use case, we created a software application (running on *Windows 11*) which allows us to use our hardware and gesture recognition to navigate through a file structure in real-time. The model prediction used for this application was the trained YOLO model, as it showed the highest accuracy among the other models. A *Python* script (version 3.10.10) was used to monitor input on the capacitive surface and, once an input was detected, the script processed the data for gesture recognition. The prediction was obtained with an average delay of 6.9 ± 1.9 s and passed the detected to the OS which reacted according to the gesture detected (See Video S2, Supporting Information). Using this application, VI users can thus navigate through folders or files on their computer using the following gestures:

- single-click to select the first file in the directory (equivalent to a single mouse click)
- swipe-right or swipe left to switch the file to the right or the left, respectively
- double-click to open the highlighted file
- (within an upon file) scroll-up and scroll-down to move through, e.g., pages of the document or pan a graphic
- audio-output of textual content of a page via the zoom-in gesture which will trigger the screen reader to read aloud the caption below the image
- zoom-out to close the file, returning the user to the directory

2.4. Prototype Testing

One of the authors, Gerhard Jaworek, a VI staff at the Center for Digital Accessibility and Assistive Technology (ACCESS Center) of Karlsruhe Institute of Technology (KIT), assessed the prototype from the standpoint of a potential future user of the device. The goal of the test was to assess the behavior of the system when employed by VI users. For the convenience of the VI user during the test, an audio output was added to the GR software. The

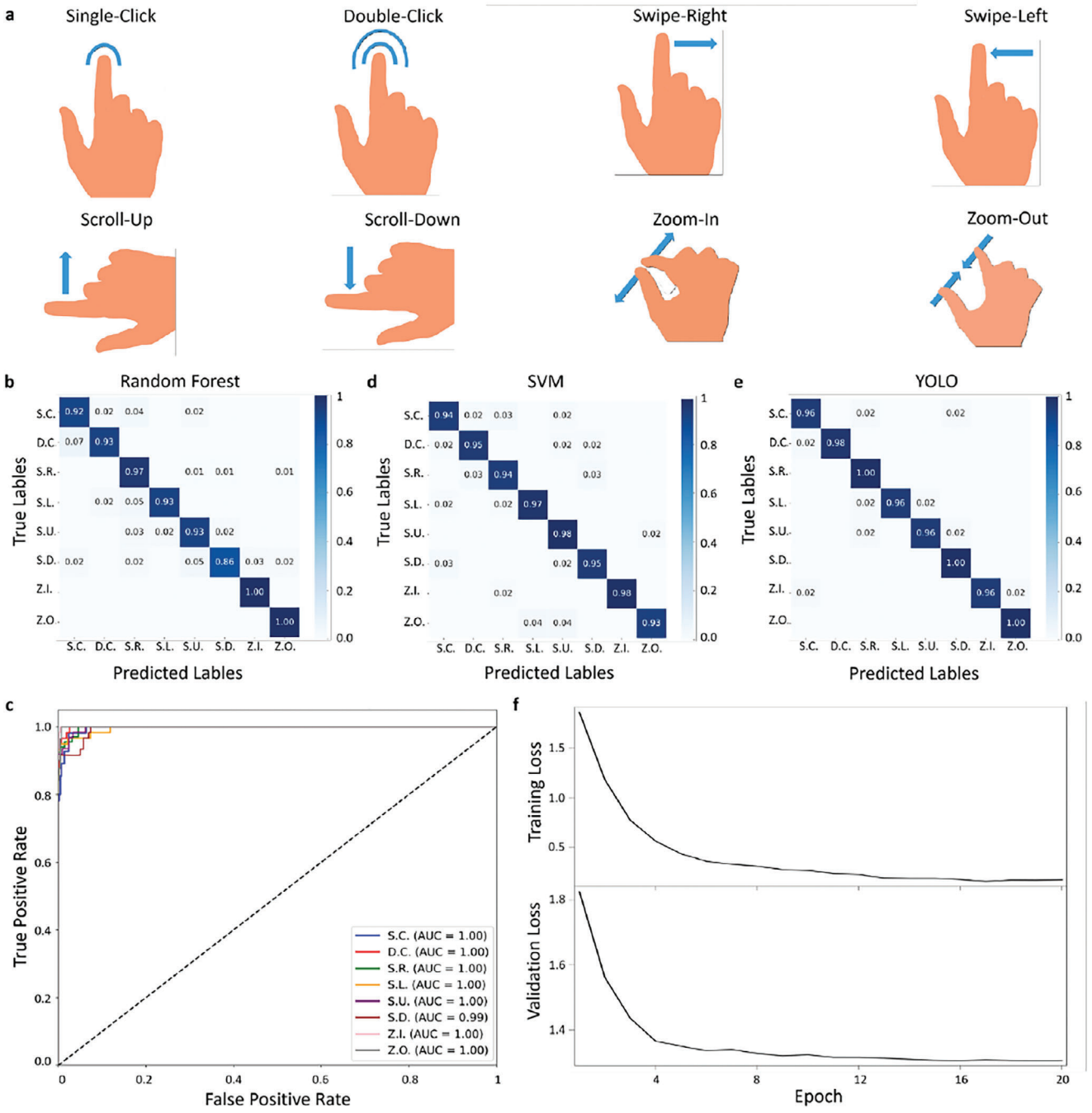

Figure 4. Resulting confusion matrices from the eight gesture classifications. a) Schematic of the gestures trained (Single-click (S.C.), double-click (D.C.), swipe-right (S.R.), swipe-left (S.L.), scroll-up (S.U.), scroll-down (S.D.), zoom-in (Z.I.), zoom-out (Z.O.)) b) The normalized confusion matrix using Random Forest with a test accuracy of 94.38%. c) The receiver operating characteristic curves of the random forest algorithm. d) The normalized confusion matrix using SVM with a test accuracy of 95.4%. e) The normalized confusion matrix using YOLOv8 with a validation accuracy of 97.76%. f) The training and validation losses of the YOLOv8 classification model.

VI user was asked to perform each gesture 5 times to provide feedback on the functionality and convenience of the CTS. The prototype device was embedded in a 3D-printed casing to avoid unintended display input by the user (Figure S2a, Supporting Information). Among five gestures, some were more difficult to detect, due to the small size of the prototype and the rough surface of the taxels. However, given such limitations, the algorithm was successful for GR at 60% with some gestures reaching detection rates as high as 80% (S.C.) and 100% (D.C.) (See Video S3, Supporting Information). Our data along with the current primary test for the prototype pave the way for the development of the presented CTS embedded into tactile displays.

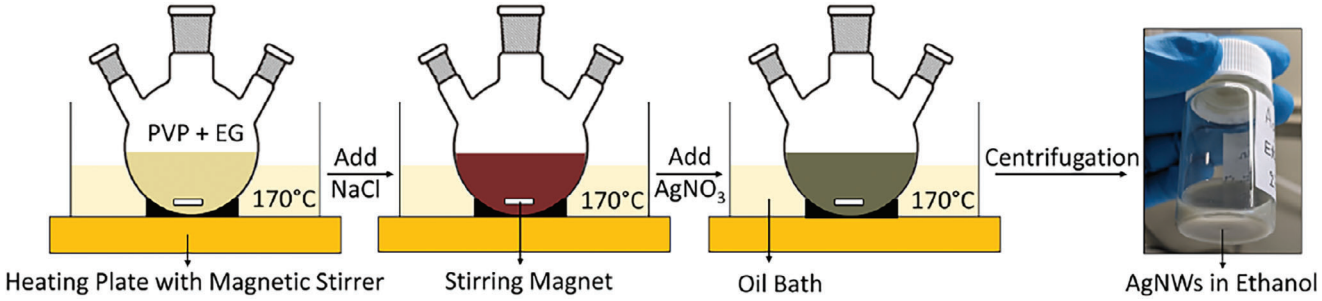

Figure 5. Schematic view of the synthesis process for the silver nanowires.

3. Conclusion

In this work, we have demonstrated the hardware implementation of a flexible and tactile capacitive screen for tactile displays based on AgNWs for generating elastic and stretchable electrodes on a multi-layer polyimide substrate. AgNWs were synthesized in a one-day process at high yield and very good reproducibility. The patterned AgNWs showed the narrow distribution of length and width of the wires, was well as high conductivity. We implemented the tactile capacitive touch on a 15 × 15 Braille dot array and demonstrated highly sensitive and stable operation during operation. Furthermore, we implemented a DL pattern recognition model based on the YOLO model which allowed us to detect gestures commonly known from the touch displays for sighted people directly interoperable with the Braille display. We showed that we can detect in real-time a total of eight gestures (single- and double-click, swipe-left and -right, scroll-up and -down as well as zoom-in and -out) allowing us to build a software application that helps a VI user operate a file system with common quality-of-life features such as, e.g., file selection, opening, closing, swiping and zooming. The validation accuracy of our model was 97.76% and proved very robust with the primary prototype testing. To further adapt this system for everyone, the data collection of all gestures should be collected from a wide range of individuals with visual impairment with more diversity in age and gender. In this way, the algorithm would be more robust to changes and will reduce substantially the misclassification.

We believe that this implementation of two technology levels, e.g., the development of a robust flexible multilayer capacitive screen suitable for adaptation to arbitrary Braille displays, in combination with the robust and fast ML model for precise gesture recognition, will be a significant step forward toward the next-generation of gesture-enabled, touch-input tactile displays for the visually impaired and advance their integration and equity into STEM fields.

4. Experimental Section

Silver Nanowire Synthesis: The process of synthesizing the AgNWs is discussed in detail elsewhere.[74] In the current work, we employed a 1-day synthesis approach where 0.334 g of PVP (360k Da Mw, Sigma Aldrich, Germany) was added to 20 mL ethylene glycol (EG) (CARL ROTH, Germany) in a triple neck flask and placed in a heated (170 °C) and stirred (500 rpm) oil bath until a clear solution was obtained. Then, 0.025 g of sodium chloride (NaCl) was added to the mixture over 3 min to initiate the silver seeding. Afterward, 0.110 g of the silver source, silver nitrate (AgNO3), was added slowly to the mixture and kept under mixing and stirring for 40 min. After cooling, the mixture was centrifuged three times (6000 rpm for 30 min) to separate the unwanted solvents from the AgNWs paste. The synthesized AgNWs paste was diluted in ethanol to obtain the final AgNWs solution. The color change was monitored as an indicator of the completion of each step during the synthesis (shown schematically in **Figure 5**).

Fabrication of the Capacitive Touch Screen: A PI film with 50 µm thickness was used as the base substrate. A PI tape (Fabistron GmbH, Germany) with 40 µm thickness and 50 mm width was used as the dielectric layer separating the electrodes, the protection layer on top, and the mask for electrode fabrication. Two PI layers were placed on top of each other, one as the base material and the other as the mask. First, a laser cutter (Protolaser U4, LPKF, Germany) was used to create a grid of holes corresponding to the Braille pins of the tactile display each with a 1.2 mm diameter and 2.54 mm pitch resulting in a 10-dpi resolution. Following the laser cut, the laser cutting was used to pattern the PI shadow mask for the horizontal diamond-shaped electrodes (Figure 1a). A total of seven passes were used during laser cutting resulting in the structuring of both layers, followed by another two passes for structuring the electrodes on the top layer. The parameters were set to 1.5 W power, 25 kHz frequency, 130 mm s^{-1} mark speed, and 15 µm laser beam diameter. Following the laser cutting, the electrode strips were removed for patterning the AgNWs structures. The surface of the PI substrates was activated by plasma cleaning (Diener Plasma Electronic, Germany) for 5 min at 0.3 mbar. Then, the AgNWs ink was spin-coated at 150 rpm for 10 s. After the spin-coating step, the PI layers with the AgNWs were placed in an oven at 135 °C for 40 min for annealing. Finally, the PI mask was removed and the AgNWs electrodes were patterned on the PI substrate underneath. The process was repeated for the vertical electrodes and a PI protective layer was placed on top of both layers. The fabrication process is shown schematically in **Figure 6**.

Touch Screen Characterization: The electrode's thickness and roughness were measured using a white light interferometer NewView 9000 (BU Zygo, Germany) to check the homogeneity of the patterned electrodes. The resistance of the electrodes was evaluated using a four-probe measurement setup. This consisted of four gold-plated spring contacts that were placed at an equal distance to each other of 5.08 mm pitch. A constant current supply of ≈12 mA was connected to the external pins, whereas a digital multi-meter was connected to the internal pins. Ten measurements were taken at different locations and the results were averaged.

Gestures Data Collection: An expansion board of type CY8CKIT-041S-MAX (Infineon, Germany) was connected to both horizontal and vertical electrodes and used for mutual capacitive sensing. The capacitance was initialized by recording the data with and without the touch for each electrode and the signal-to-noise values were obtained. The data was collected for eight gestures (single-click, double-click, swipe-right, swipe-left, scroll-up, scroll-down, zoom-in, zoom-out). Two individuals (with two different hand sizes) collected 300 measurements for each gesture to obtain more diverse data. Each measurement was acquired for 3 s with a sampling frequency of 60 Hz.

Base Plate for the Experimental Setup: The capacitive layers consist of 28 electrodes. To avoid the complexity of connecting wires to the expansion board for data collection, a PCB board was designed using EAGLE

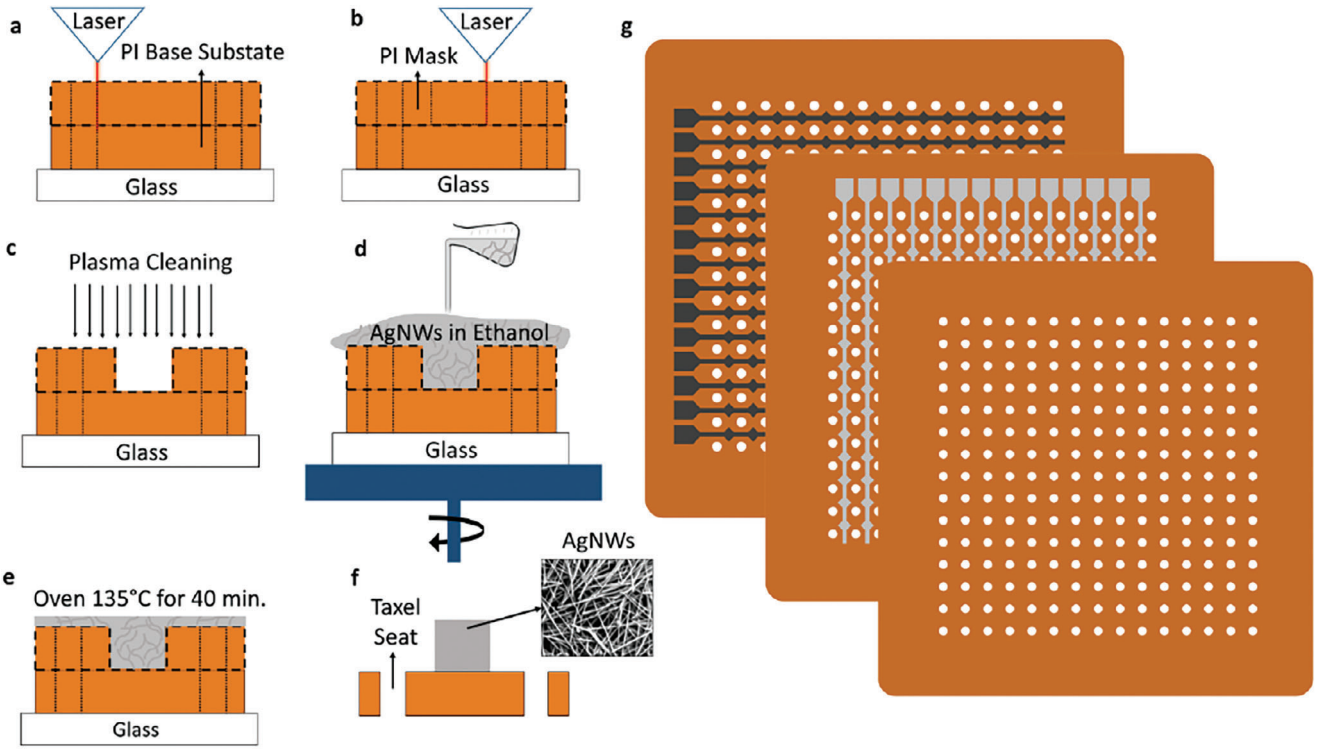

Figure 6. The fabrication process of a flexible CTS. a) Laser cutting of the grid of holes corresponding to the location and the shape of the Braille pins. b) Laser cutting of the PI mask for the electrode patterns. c) Removal of the electrode strips and plasma cleaning. d) Spin-coating of the AgNWs solution. e) AgNWs annealing and solvent evaporation. f) The resulting electrodes after the mask removal. g) The final CTS with the protective PI layer on top.

software and manufactured by Beta-Layout GmbH, Germany to connect the capacitive layers with pin headers and a flexible cable with the expansion board. The taxels' holder was designed using Autodesk Inventor software and was 3d printed using Asiga Max X (Asiga, Alexandria, NSW, Australia) with Asiga FusionGRAY resin.

Supporting Information

Supporting Information is available from the Wiley Online Library or from the author.

Acknowledgements

This work was funded by the European Research Council (ERC) under the European Union's Horizon 2020 research and innovation programme (grant agreement no. 816006). Also, this project has received funding from the Deutsche Forschungsgemeinschaft (DFG, German Research Foundation) under Germany's Excellence Strategy—EXC-2193/1-390951807. This work as well is part of the Research Cluster 25 "Interactive and Programmable Materials (IPROM)" funded by the Carl Zeiss Foundation. The authors would like to thank Nevil Khadela for helping with the silver nanowires synthesis.

Open access funding enabled and organized by Projekt DEAL.

Conflict of Interest

The authors declare no conflict of interest.

Data Availability Statement

The data that support the findings of this study are available from the corresponding author upon reasonable request.

Keywords

capacitive touch screens, hand gesture recognition, machine learning, silver nanowires, tactile displays, visually impaired equity

Received: June 26, 2024
Revised: October 21, 2024
Published online: November 9, 2024

[1] Global Tablet Market, https://www.canalys.com/newsroom/global-tablet-market-q4-2023 (accessed: February 2024).
[2] WHO-Visually Impaired, https://www.who.int/news-room/fact-sheets/detail/blindness-and-visual-impairment (accessed: August 2024).
[3] EU Market-Tablets, https://insidevision-us.com (accessed: June 2024).
[4] Metec, https://metec-ag.de/en/produkte-graphik-display.php (accessed: June 2024).
[5] P. Sharma, R. Kaur, *AIP Conf. Proceed.* **2023**, *2705*, 040002.
[6] S. Hotelling, J. Strickon, B. Huppi, (Multipoint Touchscreen), US20060097991A1, **2006**.
[7] S. Mascetti, C. Bernareggi, M. Belotti, in *The Proceedings of the 13th International ACM SIGACCESS Conference on Computers and Accessibility*, Association For Computing Machinery, New York, NY **2011**, pp. 295–296.
[8] E. Mattheiss, G. Regal, J. Schrammel, M. Garschall, M. Tscheligi, *J. Assist. Technol.* **2015**, *9*, 147.
[9] M. Alnfiai, S. Sampalli, *Proc. Comput. Sci.* **2017**, *109*, 257.
[10] R. S. Cok, R. P. Bourdelais, C. J. Kaminsky, (Flexible Resistive Touch Screen), US7081888B2, **2006**.

[11] C.-C. Wu, *RSC Adv.* **2018**, *8*, 11862.
[12] D. S. Hecht, D. Thomas, L. Hu, C. Ladous, T. Lam, Y. Park, G. Irvin, P. Drzaic, *J. Soc. Inform. Display.* **2009**, *17*, 941.
[13] G. Eda, G. Fanchini, M. Chhowalla, *Nat. Nanotech.* **2008**, *3*, 270.
[14] T. Mochizuki, Y. Takigami, T. Kondo, H. Okuzaki, *J. Appl. Polym. Sci.* **2018**, *135*, 45972.
[15] J. Cameron, P. J. Skabara, *Mater. Horiz.* **2020**, *7*, 1759.
[16] Y. Liu, J. Liu, H. Lin, L. Zeng, in *2020 IEEE Int. Conf. on Signal Processing, Communications and Computing (ICSPCC)*, IEEE, Macau, China **2020**, pp. 1–5.
[17] T. Nara, M. Takasaki, T. Maeda, T. Higuchi, S. Ando, S. Tachi, *IEEE Comput. Grap. Appl.* **2001**, *21*, 56.
[18] A. L. Pang, A. Arsad, M. Ahmadipour, *Polym. Adv. Technol.* **2021**, *32*, 1428.
[19] H. Kim, A. A. Abdala, C. W. Macosko, *Macromolecules.* **2010**, *43*, 6515.
[20] T. Y. Choi, B.-U. Hwang, B.-Y. Kim, T. Q. Trung, Y. H. Nam, D.-N. Kim, K. Eom, N.-E. Lee, *ACS Appl. Mater. Interfaces.* **2017**, *9*, 18022.
[21] K. Hu, D. D. Kulkarni, I. Choi, V. V. Tsukruk, *Prog. Polym. Sci.* **2014**, *39*, 1934.
[22] P. Cataldi, S. Dussoni, L. Ceseracciu, M. Maggiali, L. Natale, G. Metta, A. Athanassiou, I. S. Bayer, *Adv. Sci.* **2018**, *5*, 1700587.
[23] C. Yu, C. Masarapu, J. Rong, B. Wei, H. Jiang, *Adv. Mater.* **2009**, *21*, 4793.
[24] S. Zhang, M. Zhou, M. Liu, Z. H. Guo, H. Qu, W. Chen, S. C. Tan, *Nat. Commun.* **2023**, *14*, 3245.
[25] S. Zhang, Y. Deng, A. Libanori, Y. Zhou, J. Yang, T. Tat, L. Yang, W. Sun, P. Zheng, Y.-L. Zhu, J. Chen, S. C. Tan, *Adv. Mater.* **2023**, *35*, 2207916.
[26] Y. Li, S. Guo, B. Wang, J. Sun, L. Zhao, T. Wang, X. Yan, F. Liu, P. Sun, J. Wang, S. C. Tan, G. Lu, *InfoMat.* **2024**, *6*, e12544.
[27] D. Fu, R. Yang, Y. Wang, R. Wang, F. Hua, *Adv. Mater. Technol.* **2022**, *7*, 2200027.
[28] A. Elsokary, M. Soliman, F. Abulfotuh, S. Ebrahim, T. Sadat-Shafai, M. Karim, *Sci. Rep.* **2024**, *14*, 3045.
[29] W. Li, A. Meredov, A. Shamim, *npj Flex Electron.* **2019**, *3*, 19.
[30] T. Paek, D. M. Chickering, *User Model User-Adap. Inter.* **2007**, *17*, 93.
[31] S. Brewster, *Personal Ub Comp.* **2002**, *6*, 188.
[32] S. M. Aslam, S. Samreen, *IEEE Access.* **2020**, *8*, 127560.
[33] S. Shokat, R. Riaz, S. S. Rizvi, A. M. Abbasi, A. A. Abbasi, S. J. Kwon, *Human-Centric Comput. Inform. Sci.* **2020**, *10*, 41.
[34] X. Gao, J. Zhang, Z. Wei, in *2018 IEEE 15th Int. Conf. on Networking, Sensing and Control (ICNSC)*, IEEE, Zhuhai **2018**, pp. 1–6.
[35] F. Vidal-Verdu, M. Hafez, *IEEE Trans. Neural Syst. Rehabil. Eng.* **2007**, *15*, 119.
[36] M. Nadeem, N. Aziz, U. Sajjad, F. Aziz, H. Shaikh, *International Conference on Advanced Robotics and Mechatronics (ICARM), IEEE* **2016**.
[37] P. Chakraborti, H. A. K. Toprakci, P. Yang, N. Di Spigna, P. Franzon, T. Ghosh, *Sens. Actuators, A.* **2012**, *179*, 151.
[38] A. Bhowmick, S. M. Hazarika, *J Multimodal User Interfaces.* **2017**, *11*, 149.
[39] W. Yang, J. Huang, R. Wang, W. Zhang, H. Liu, J. Xiao, *IEEE Trans. Haptics.* **2021**, *14*, 712.
[40] S. Bhagwat, C. O'Brien, A. Hamza, S. Sharma, C. Rein, M. Sanjaya, D. Helmer, F. Kotz-Helmer, P. Pezeshkpour, B. E. Rapp, *Adv. Mater.* **2022**, *34*, 2201469.
[41] D. Chen, Y. Zhang, X. Hu, G. Chen, Y. Fang, X. Chen, J. Liu, A. Song, *IEEE Trans. Neural Syst. Rehabil. Eng.* **2024**, *32*, 934.
[42] A. Hamza, A. Navale, Q. Song, S. Bhagwat, F. Kotz-Helmer, P. Pezeshkpour, B. E. Rapp, *Biomed. Microdevices.* **2024**, *26*, 14.
[43] W.-B. Zhao, J.-J. Zhu, H.-Y. Chen, *J. Cryst. Growth.* **2003**, *258*, 176.
[44] B. H. Hong, S. C. Bae, C.-W. Lee, S. Jeong, K. S. Kim, *Science.* **2001**, *294*, 348.
[45] J.-J. Zhu, Q.-F. Qiu, H. Wang, J.-R. Zhang, J.-M. Zhu, Z.-Q. Chen, *Inorg. Chem. Commun.* **2002**, *5*, 242.
[46] D. Zhang, L. Qi, J. Yang, J. Ma, H. Cheng, L. Huang, *Chem. Mater.* **2004**, *16*, 872.
[47] J. Choi, Y. S. Shim, C. H. Park, H. Hwang, J. H. Kwack, D. J. Lee, Y. W. Park, B.-K. Ju, *Small.* **2018**, *14*, 1702567.
[48] G. Namgung, Q. Thanh Hoai Ta, W. Yang, J-S. Noh, *ACS Appl. Mater. Interfaces* **2018**, *11*, 1.
[49] S. Kang, T. Kim, S. Cho, Y. Lee, A. Choe, B. Walker, S.-J. Ko, J. Y. Kim, H. Ko, *Nano Lett.* **2015**, *15*, 7933.
[50] A. R. Madaria, A. Kumar, C. Zhou, *Nanotechnology.* **2011**, *22*, 245201.
[51] X. Xu, G. Han, H. Yu, X. Jin, J. Yang, J. Lin, C. Ma, *J. Phys. D: Appl. Phys.* **2019**, *53*, 05LT02.
[52] J. Liang, K. Tong, Q. Pei, *Adv. Mater.* **2016**, *28*, 5986.
[53] Y. Sun, B. Gates, B. Mayers, Y. Xia, *Nano Lett.* **2002**, *2*, 165.
[54] D. Tan, C. Jiang, Q. Li, S. Bi, J. Song, *J. Mater. Sci.: Mater. Electron.* **2020**, *31*, 15669.
[55] R. R. da Silva, M. Yang, S.-I. Choi, M. Chi, M. Luo, C. Zhang, Z.-Y. Li, P. H. C. Camargo, S. J. L. Ribeiro, Y. Xia, *ACS Nano.* **2016**, *10*, 7892.
[56] A. Nekahi, S. P. H. Marashi, D. H. Fatmesari, *Mater. Chem. Phys.* **2016**, *184*, 130.
[57] J.-J. Zhu, C.-X. Kan, J.-G. Wan, M. Han, G.-H. Wang, *J. Nanomater.* **2011**, *2011*, 1.
[58] Y. Jiang, R. Tao, H. Zhang, N. Wan, Y. Yang, D. Gu, T. Zhang, Y. Rui, J. Xu, *J. Mater. Sci.: Mater. Electron.* **2023**, *34*, 26.
[59] A. Sivan Pillai, S. Sudhakar, S. Benny, S. Sahoo, A. Chandran, S. Kuzhichalil Peethambharan, *J. Mater. Chem. C.* **2024**, *12*, 575.
[60] https://www.infineon.com, https://www.cypress.com, PSoC™ 4 and PSoC™ 6 MCU CAPSENSE™ (accessed: April 2024).
[61] S. S. Sankar, S. Kovar, S. S. Sankar, S. Kovar, in 2024 IEEE Joint International Symposium on Electromagnetic Compatibility, IEEE, Ginowan, Okinawa **2024**, pp. 300–303.
[62] L. Wang, *Support Vector Machines: Theory and Applications*, Springer Science & Business Media, Berlin, Heidelberg **2005**.
[63] W. S. Noble, *Nat. Biotechnol.* **2006**, *24*, 1565.
[64] D. A. Pisner, D. M. Schnyer, in *Machine Learning* (Eds.: A. Mechelli, S. Vieira), Academic Press, Cambridge, MA **2020**, pp. 101–121.
[65] Y. Liu, Y. Wang, J. Zhang, in *Information Computing and Applications* (Eds.: B. Liu, M. Ma, J. Chang), Springer, Berlin, Heidelberg **2012**, pp. 246–252.
[66] G. Biau, E. Scornet, *TEST.* **2016**, *25*, 197.
[67] A. Parmar, R. Katariya, V. Patel, in International Conference on Intelligent Data Communication Technologies and Internet of Things (ICICI) 2018, Springer International Publishing, Cham, **2019**, pp. 758–763.
[68] G. Jocher, A. Chaurasia, J. Qiu,"Ultralytics YOLO (Version 8.0.0)[Computer software]", https://github.com/ultralytics/ultralytics **2023**.
[69] J. Terven, D.-M. Córdova-Esparza, J.-A. Romero-González, *Mach. Learn. Knowl. Extract.* **2023**, *5*, 1680.
[70] J. Redmon, S. Divvala, R. Girshick, A. Farhadi, in 2016 IEEE Conference on Computer Vision and Pattern Recognition *(CVPR)*, *IEEE* **2016**, pp. 779–788.
[71] N. Ketkar, J. Moolayil, in *Deep Learning with Python: Learn Best Practices of Deep Learning Models with PyTorch* (Eds.: N. Ketkar, J. Moolayil), Apress, Berkeley, CA **2021**, pp. 197–242.
[72] Z. Li, F. Liu, W. Yang, S. Peng, J. Zhou, *IEEE Trans. Neural Netw. Learn. Syst.* **2022**, *33*, 6999.
[73] R. Chauhan, K. K. Ghanshala, R. C. Joshi, in *2018 First International Conference on Secure Cyber Computing and Communication (ICSCCC), IEEE* **2018**, pp. 278–282.
[74] L. Hu, H. S. Kim, J.-Y. Lee, P. Peumans, Y. Cui, *ACS Nano.* **2010**, *4*, 2955.